CCS Chemistry

COMMUNICATION

Received: June 3, 2021 | Accepted: Sept. 15, 2021 | Published: Oct. 12, 2021

Porous Pyrene Organic Cage with Unusual Absorption Bathochromic-Shift Enables Visible Light Photocatalysis

Nana Sun[1†], Dongdong Qi[1†], Yucheng Jin[1], Hailong Wang[1]*, Chiming Wang[1], Chen Qu[1], Jiemin Liu[1], Yinghua Jin[2], Wei Zhang[2]* & Jianzhuang Jiang[1]*

[1]*Beijing Advanced Innovation Center for Materials Genome Engineering, Beijing Key Laboratory for Science and Application of Functional Molecular and Crystalline Materials, Department of Chemistry and Chemical Engineering, School of Chemistry and Biological Engineering, University of Science and Technology Beijing, Beijing 100083,* [2]*Department of Chemistry, University of Colorado, Boulder, CO 80309*

**Corresponding authors: hlwang@ustb.edu.cn; wei.zhang@colorado.edu; jianzhuang@ustb.edu.cn;* †N. Sun and D. Qi contributed equally to this work.

Cite this: *CCS Chem.* **2022**, 4, 2588–2596
DOI: 10.31635/ccschem.021.202101202

We have constructed a novel porous pyrene-based organic cage, PyTC1, through the condensation reaction of cyclohexanediamine with 5,5′-(pyrene-1,6-diyl) diisophthalaldehyde. Single-crystal X-ray diffraction analysis reveals the effective intercage C–H···π interaction between cyclohexanediimine and pyrene segments. Such a soft intercage C–H···π interaction, rather than a classic *J*-aggregate with slipped π–π-stacking configuration, induced an unusual bathochromic shift of pyrene-based chromophore absorption from an ultraviolet region of PyTC1 in solution to the visible light region of PyTC1 in solid-state. This enabled heterogeneous visible light photocatalysis of aerobic hydroxylation of benzeneboronic acid derivatives. To the best of our knowledge, this is the first report that represents an absorption bathochromic shift caused by C–H···π interaction. Such phenomenon could endow visible-light-driven photocatalysis that originally could only be achieved using UV light with the same chromophore.

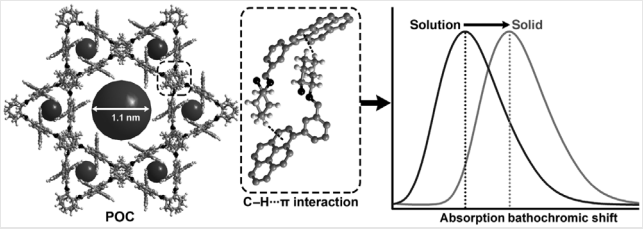

Keywords: **absorption bathochromic-shift, *J*-aggregate, porous organic cage, pyrene derivatives, visible light catalysis**

Introduction

Supramolecular chemistry offers a powerful toolkit to assemble well-defined and predictable structures from molecules by using noncovalent interactions.[1–3] Supramolecular materials that self-assemble from versatile molecular building blocks have been exploited in many vital applications, including organic field-effect transistors, organic light-emitting diodes (LEDs), light-harvesting, molecular machines, sensors, gas absorption, catalysis, and drug delivery.[4–13] The functionalities of molecular superstructures are strongly dependent on the intermolecular packing because of the strong coupling between the electronic and structural dynamics of the molecular units

DOI: 10.31635/ccschem.021.202101202
Corrected Citation: *CCS Chem.* **2022**, 4, 2588–2596
Previous Citation: *CCS Chem.* **2021**, 3, 2917–2921
Link to VoR: https://doi.org/10.31635/ccschem.021.202101202

in the solid state. In particular, the electron transport,[5] fluorescence,[6] and electronic absorption[14,15] of solid assemblies from conjugated molecules are strongly associated with aggregated structures. For example, the parallel aligned aromatic chromophores in various supramolecular assemblies with tilt angle (θ) <54.78° (*J*-aggregate definition) allow electronic excitation from the ground state to the excited state with lower energy relative to the monomeric molecules, resulting in an absorbance bathochromic-shift (Scheme 1a).[14] Although supramolecular chemistry has progressed tremendously in the past 50 years, this discipline is still very active and faces many yet unexplored territories beyond the monomeric molecular properties.

The development of high-performance photoredox catalysts for organic transformations is of great significance because they can overcome the high energy barrier for conventional activation of organic molecules and realize new and significant transformations under mild conditions.[16–19] The direct/indirect use of relatively low-energy visible light is highly preferred in photoredox catalysis in order to realize more energy-efficient and green organic transformations and minimize damage during photocatalysis. Polycyclic aromatic hydrocarbons (PAHs) with high redox potentials have been recognized as excellent photoredox catalysts. However, PAHs generally absorb high-energy ultraviolet light, which has impeded their wide practical applications in photoredox catalysis.[20,21]

Porous organic cages (POCs) constructed from covalently linked molecular building blocks have emerged as new types of nanosized synthons for porous reticular frameworks.[22–29] In comparison with other porous materials,[30–46] POCs possess both intrinsic intracage cavity and intercage porosity upon assembly, in addition to their advantageous solution processability and regeneration through recrystallization. The unique porous nature of POCs can facilitate the mass transfer of reactants and products in heterogeneous catalysis.[47–59] Moreover, the arrangement of chromophores within a cage and the assembly could tune their light-harvesting wavelength and utilization efficiency depending on the aggregation model. In this work, we demonstrate the first example of

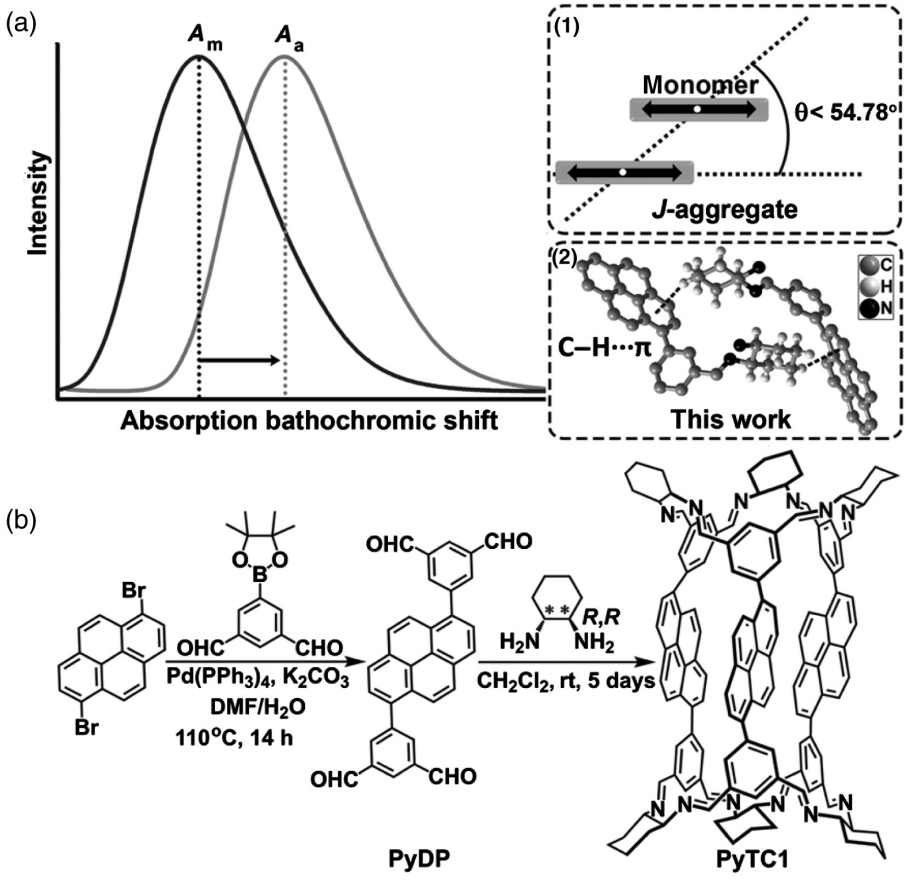

Scheme 1 | *(a) Illustration of absorbance bathochromic shift due to the (1) conventional J-type aggregation and (2) C–H···π interaction between neighboring aromatic chromophores unveiled in this work (A_m and A_a represent the absorption maximum of monomeric molecule and assembly, respectively). (b) Synthesis of PyTC1 through imine condensation.*

DOI: 10.31635/ccschem.021.202101202
Corrected Citation: *CCS Chem.* **2022**, 4, 2588–2596
Previous Citation: *CCS Chem.* **2021**, 3, 2917–2921
Link to VoR: https://doi.org/10.31635/ccschem.021.202101202

an unusual C–H···π interaction-induced absorption bathochromic shift in POCs (denoted as PyTC1) upon their self-assembly in the solid-state (Scheme 1). The adsorption of the solid-state supramolecular assembly of PyTC1 is shifted to the visible light region due to the C–H···π interactions between neighboring POC molecules, which is in great contrast to the ultraviolet absorption of its solution sample in CH_2Cl_2. This endows the PyTC1 supramolecular assembly with the prominent heterogeneous visible light photocatalytic activity for aerobic hydroxylation of benzeneboronic acid derivatives, with yields almost five times higher than that of the reaction catalyzed by the same Py chromophore but without C–H···π interaction. Thus, our study opens many new possibilities for engineering the absorption properties of PAHs with high redox potentials to realize more energy-efficient and greener photocatalysis under visible light by incorporating them in rigid POC molecules.

Results and Discussion

Inspired by the high redox potentials of PAHs able to drive many photoredox reactions,[20,21] 1,6-pyrene derivative was introduced into a [3+6]-type organic cage (denoted as PyTC1). In details, the Suzuki–Miyaura cross-coupling reaction of 1,6-dibromopyrene and 5-(4,4,5,5-tetramethyl-1,3,2-dioxaborolan-2-yl)isophthalaldehyde afforded a tetraaldehyde cage precursor 5,5′-(pyrene-1,6-diyl)diisophthalaldehyde (PyDP) in the presence of Pd$(PPh_3)_4$ as a catalyst. PyTC1 was formed as a pure pale yellow solid in high yield (70%) through the [3+6] cycloimination reaction of PyDP with cyclohexanediamine (Scheme 1b). The PyTC1 obtained was characterized with various techniques, including NMR spectroscopy, mass spectrometry, and single-crystal X-ray diffraction (Figure 1 and Supporting Information Figures S1–S3 and Table S1).

The crystal structure of PyTC1 revealed three 1,6-pyrene units bridged by six cyclohexanediimine segments, arranged in a triangular shape with a side length of 1.6 nm, forming a tubular structure with a length of 2.4 nm (Figures 1a and 1b and Supporting Information Table S1). The nearest distance between the hydrogen atom of 1,6-pyrene to the neighboring 1,6-pyrene plane was 2.93 Å, indicating the existence of weak interactions. The adjacent molecules were connected by intercage C–H···π interactions between the H atoms of cyclohexanediimine and the center benzene ring of the pyrene units, as indicated by the short distances of 2.865 and 2.984 Å,

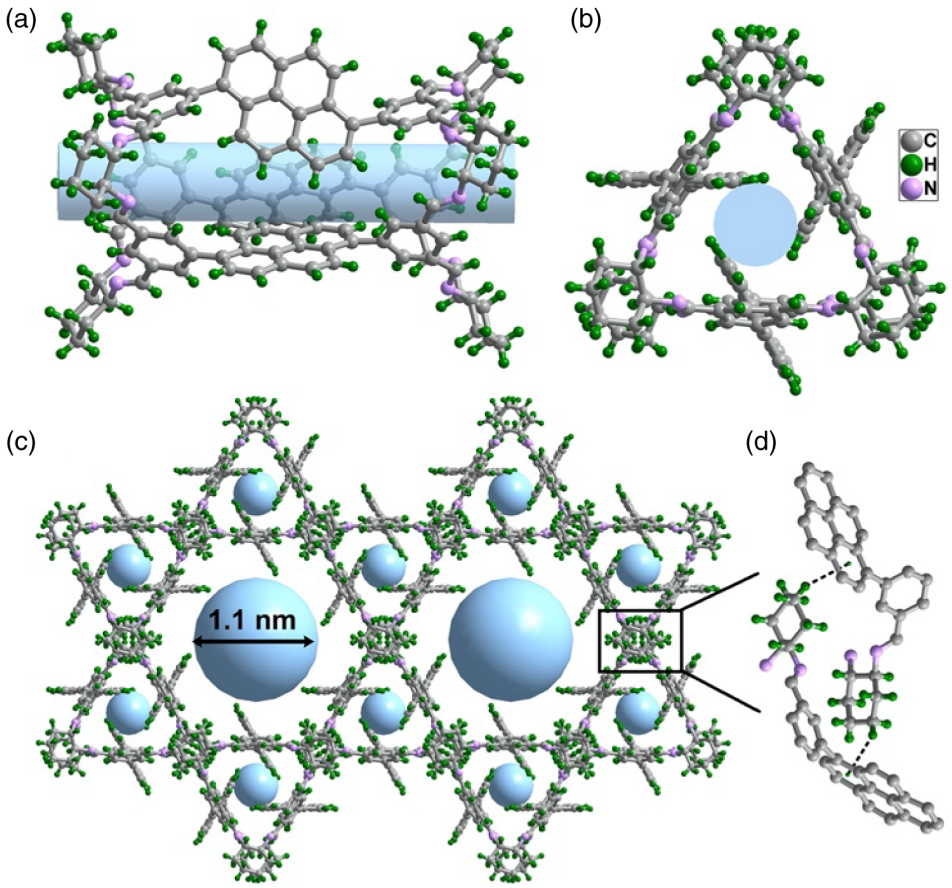

Figure 1 | *Structure of PyTC1. (a) Side view. (b) Top view. (c) Packing structure showing one-dimensional channels as cyan balls. (d) Intercage C–H···π interaction (black dash line).*

DOI: 10.31635/ccschem.021.202101202
Corrected Citation: *CCS Chem.* **2022**, 4, 2588–2596
Previous Citation: *CCS Chem.* **2021**, 3, 2917–2921
Link to VoR: https://doi.org/10.31635/ccschem.021.202101202

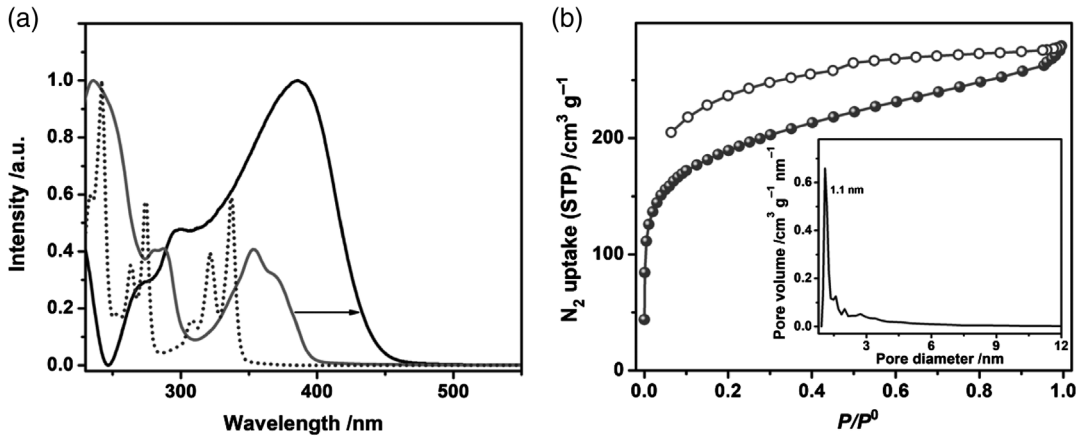

Figure 2 | *(a) Solid-state UV–vis diffuse reflectance spectra of PyTC1 (black) and solution UV–vis spectra of PyTC1 (grey) and pyrene (dot line) in CH_2Cl_2. (b) N_2 sorption isotherms of PyTC1 at 77 K (inset: pore size distribution based on DFT calculation).*

forming a porous supramolecular framework with a bigger pore size of ~1.1 nm (Figures 1c and 1d).

The electronic absorption spectrum of the solution of PyTC1 in CH_2Cl_2 showed maximum absorption at 236 nm and other two medium adsorption bands at 288 and 354 nm (Figure 2a). Upon excitation at 350 nm (λ_{ex}), the emission spectrum of PyTC1 in CH_2Cl_2 displayed a maximum emission at 404 nm with a fluorescence quantum yield Φ = 47% and a lifetime τ = 2.97 ns (Supporting Information Figures S4 and S5). For the solid sample of PyTC1, the maximum absorption appeared at 385 nm with the band ending at 480 nm, which demonstrated a significant bathochromic shift, compared with PyTC1 in solution (Figure 2a). It is worth noting that the bathochromic-shifted absorption band of dye aggregates relative to that of the monomer has been generally assigned to *J*-aggregates.[14] Interestingly, the packing structure of PyTC1 did not show any *J*-aggregate feature for pyrene chromophores (Figure 1), precluding the origin of the observed absorption bathochromic shift from *J*-aggregation. Therefore, we attributed the bathochromic shift observed in the solid sample of PyTC1 to the intercage C–H···π interaction. Further evidence to support the role of C–H···π interaction came from the crystal structures of pyrene (Py) and a small molecule model compound, 1,1′,1″,1‴-(pyrene-1,6-diylbis(benzene-5,1,3-triyl))tetrakis(*N*-cyclohexylmethanimine) (PyTM) (Supporting Information Figures S24–S26 and Scheme S1), displaying bathochromic-shift in the absorption bands of their solid samples in comparison with those of the solution samples (Supporting Information Figures S6–S9). Notably, in addition to the C–H···π interactions between the neighboring pyrene molecules, *H*-type aggregation of pyrene dimers through π···π interaction with a tilted angle of 63.18° was also found in the crystal structure, which should lead to a blue shift (Supporting Information Figure S6).[14] The observed bathochromic shift in the solid sample of pyrene, therefore, suggests that C–H···π interactions overshadowed the π···π interactions between *H*-aggregated pyrene dimers.

The bathochromic absorption shift of PyTC1 in the solid-state relative to the spectra of PyTC1 in solution was further examined through the theoretical simulations on the basis of time-dependent density functional theory (TDDFT) with Tamm–Dancoff approximation (TDA). For PyTC1 in CH_2Cl_2, very broadband appeared between 300 and 400 nm. The second-order differentiation was performed to find the absorption signals, revealing four overlapping bands centered at 385, 374, 353, and 337 nm (Supporting Information Figure S10). According to the TDDFT results, the transitions of $HOMO_{(pyrene)}$/$HOMO\text{-}1_{(pyrene)}$ → $LUMO_{(pyrene)}$/$LUMO+1_{(pyrene)}$ (HOMO = highest occupied molecular, LUMO = lowest unoccupied molecular) led to bands at 341, 382, and 393 nm, consistent with the experimental bands at 337 and 385 nm. The transitions between pyrene units and benzene rings, namely, $HOMO_{(pyrene)}$ → $LUMO_{(benzene)}$ and $HOMO\text{-}1_{(pyrene)}$ → $LUMO+1_{(benzene)}$, yielded the bands at 370 and 354 nm, respectively (Supporting Information Table S2). The present theoretical simulation results explained well the observed bands at 337, 353, 374, and 385 nm in the second-order differentiation curve of electronic absorption of PyTC1 in CH_2Cl_2. The self-assembly of PyTC1 enabled the C–H···π interactions between cyclohexanediimine and pyrene segments; thus, the electronic absorption of the solid material originated from both the intramolecular and intermolecular electronic transitions (Supporting Information Figure S11). Although the exact details of the intermolecular electronic transitions could be fairly complicated, we managed to calculate the electron density transfer transitions possibility between the $HOMOs_{(pyrene)}$ → $LUMOs_{(pyrene)}$ transition from the adjacent cage molecules, which gave new bands with

DOI: 10.31635/ccschem.021.202101202
Corrected Citation: *CCS Chem.* **2022**, 4, 2588–2596
Previous Citation: *CCS Chem.* **2021**, 3, 2917–2921
Link to VoR: https://doi.org/10.31635/ccschem.021.202101202

relatively longer wavelengths at 380 and 357 nm due to the HOMO-$3_{(pyrene)}$ → LUMO+$1_{(pyrene)}$ and HOMO-$4_{(pyrene)}$ → LUMO+$2_{(pyrene)}$ transition, respectively (Supporting Information Figures S12 and S13 and Table S3). These results further provided evidence that the present bathochromic shift of the absorption could be attributed to the C–H···π interactions between the aromatic chromophores of the dimeric aggregates.

Nitrogen sorption isotherm at 77 K unveiled the porous nature of PyTC1, showing a Brunauer–Emmett–Teller (BET) surface area of 695 $m^2\ g^{-1}$ (Figure 2b and Supporting Information Figure S14). The pore size was estimated to be 1.1 nm (inset of Figure 2b), consistent with the intercage pore size, according to the crystal structure. The porosity, together with visible light absorption of PyTC1 solid, suggested its potential for heterogeneous photoredox catalysis. The observation by quartet electron spin resonance (ESR) signals for PyTC1 with the trapping agent, 5,5-dimethyl-1-pyrroline *N*-oxide, under the illumination of a blue LED lamp, suggested its capability of promoting superoxide anion radical $(O_2^{\bullet})^-$ evolution via visible-light-driven electron transfer process (Supporting Information Figures S15 and S16), due to the high reduction potential of PyTC1 [–1.60 V vs standard hydrogen electrode (SHE)].[56] Visible light-driven aerobic hydroxylation of benzeneboronic acid in the presence of PyTC1 photoredox catalyst under air was selected as a model reaction (Table 1).[60-64] We chose co-solvent CD_3CN/D_2O as the reaction medium, where dry PyTC1 crystals as photocatalyst had negligible solubility and presented as a solid, according to our NMR spectral data (Supporting Information Figure S17).

Upon the blue LED light illumination, benzeneboronic acid in CD_3CN/D_2O was transformed into the corresponding product (phenol) within 5.0 h with 99% conversion. PyTC1 exhibited excellent stability, showing almost the same ^1H NMR spectrum before and

Table 1 | *Visible Light-Driven Aerobic Hydroxylation of Benzeneboronic Acid Derivatives to Phenols under Various Conditions*[a]

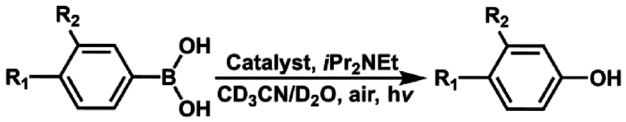

Entry	$-R_1$	$-R_2$	Catalyst	Time (h)	Conv. (%)[b]
1	–H	–H	PyTC1	5.0	>99
2	–H	–H	PyTC1	5.0	>99[c]
3	–H	–H	PyTC1	5.0	18[d]
4	–H	–H	PyTM	5.0	31[e]
5	–H	–H	Py	5.0	19[f]
6	–H	–H	None	5.0	N.D.[g]
7	–H	–H	PyTC1	5.0	N.D.[h]
8	–H	–H	PyTC1	5.0	54[i]
9	–H	–H	Py	5.0	50[i]
10	–H	–H	None	5.0	N.D.[i]
11	–CHO	–H	PyTC1	4.0	>99
12	$-CH_3$	–H	PyTC1	6.0	>99
13	$-OCH_3$	–H	PyTC1	6.0	>99
14	–H	$-OCH_3$	PyTC1	8.0	>99
15	$--OCH_3$	$-OCH_3$	PyTC1	6.0	>99
16	–Br	–H	PyTC1	6.0	>99
17	$-COOC_2H_5$	–H	PyTC1	8.0	>99

[a] Reaction conditions: benzeneboronic acid derivatives (60.0 μmol), PyTC1 (4.0 μmol), $^iPr_2NEt$ (300.0 μmol), CD_3CN (0.8 mL), and D_2O (0.2 mL) upon the irradiation of a 25 W blue LED light (420 nm < λ < 500 nm) under air.
[b] Conversion was determined by ^1H NMR spectral analysis.
[c] Under O_2.
[d] Under N_2.
[e] PyTM (12.0 μmol).
[f] Py (12.0 μmol).
[g] N.D. = not detected.
[h] In the absence of irradiation.
[i] Upon the irradiation of a 25 W UV light (350 nm < λ < 400 nm).

DOI: 10.31635/ccschem.021.202101202
Corrected Citation: *CCS Chem.* **2022**, 4, 2588–2596
Previous Citation: *CCS Chem.* **2021**, 3, 2917–2921
Link to VoR: https://doi.org/10.31635/ccschem.021.202101202

after the photocatalysis (Supporting Information Figure S18). The control experiments, conducted in the absence of air, PyTC1, or irradiation, but under otherwise identical conditions, showed lower conversion or no product formation, revealing the critical role of O_2, PyTC1 photoredox catalyst, and irradiation in the benzeneboronic acid hydroxylation process (Table 1). Note that when Py was used as the catalyst, the conversion of benzeneboronic acid was markedly slowed down even with a catalyst loading three times higher than that of the solid PyTC1 under otherwise the same experimental conditions (Figure 3). In contrast, upon the UV light illumination, both PyTC1 and Py as catalysts yielded similar conversion (54% vs 50%). These results clearly indicated the superiority of the solid pyrene-based POC in heterogeneous visible light photoredox catalysis enabled by the C–H···π interaction-induced absorption bathochromic shift. We found that the nonporous reference compound PyTM with similar visible light absorption to PyTC1 exhibits poor photocatalytic performance. The photocatalytic performances of both nonporous Py and PyTM are inferior to that of PyTC1 in the same heterogeneous system (Table 1 and Supporting Information Figure S19), further supporting the positive role of porous nature for cage-based heterogeneous photocatalyst.[65] Under the optimal reaction conditions with PyTC1 as the catalyst under air at room temperature, visible-light-driven aerobic hydroxylation of the benzeneboronic acid derivatives produced the corresponding products with high conversion of above 99%, evidently demonstrating the high photocatalytic activity of PyTC1 (Table 1). For benzeneboronic acid with –CHO substitution at the *para*-position, the reaction time for obtaining above 99% conversion reduced from 5 to 4.0 h, indicating the activating role of the electron-withdrawing group. Introducing electron-donating groups of $-CH_3$, $-OCH_3$, –Br, and $-COOC_2H_5$ substituent on the *para*- or *meta*-position of benzeneboronic acids prolonged the reaction time (up to 8.0 h) to afford a conversion above 99%. The calculated turnover number (TON) (15) of PyTC1 was comparable to that of other photocatalysts employing the same benzeneboronic acid as the substrate; these include DhaTph-Ni (TON = 10, based on active molecule sites) and LZU-190 (TON = 12, based on active molecule sites).[63,64] Moreover, a visible-light-driven aerobic hydroxylation reaction of benzeneboronic acid was carried out for five consecutive cycles. We observed constant high conversions of the substrate for all five cycles, indicating the high stability of the PyTC1 catalyst (Supporting Information Figure S20). The photocatalysis mechanism proposed is outlined in Supporting Information Figure S21. After the photocatalysis under the same reaction conditions, the BET surface area of used PyTC1 was reduced to 450 $m^2\ g^{-1}$ due to the collapsed porosity during the catalytic process (Supporting Information Figures S22 and S23).

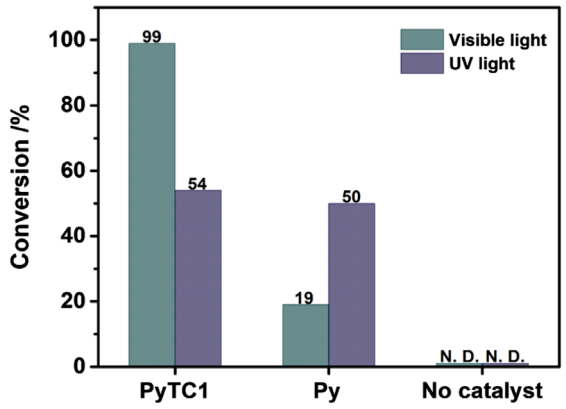

Figure 3 | *The conversion of light-driven aerobic hydroxylation of benzeneboronic acid by PyTC1 and Py was determined by ^1H NMR spectra. Reaction conditions: benzeneboronic acid (60.0 μmol), catalyst (12.0 μmol for the pyrene-based unit), $^iPr_2NEt$ (300.0 μmol), CD_3CN (0.8 mL), and D_2O (0.2 mL) with blue LED and UV light (350 nm < λ < 400 nm) irradiation for 5.0 h under air at room temperature.*

Conclusion

We have constructed and fully characterized a porous pyrene organic cage, PyTC1. With the platform of this organic cage, we revealed for the first time that soft C–H···π interactions between POC molecules could induce an unusual electronic absorption shift from the UV region for solution phase to the visible light region in the solid state, which, in turn, realized the utilization of visible light energy in photoredox catalysis. Such a phenomenon could enable visible-light-driven photocatalysis that, originally, could only be achieved using UV light with the same chromophore. These interesting findings open new possibilities for rational design and synthesis of PAH-based molecular architectures and study their self-assembly behaviors to achieve unprecedented optoelectronic and catalytic properties.

Supporting Information

Supporting Information is available and includes experimental details, NMR spectra, ESR spectra, and theoretical calculations, as well as crystallographic data for PyTC1, PyTM, and Py (CIF).

Conflict of Interest

There is no conflict of interest to report.

DOI: 10.31635/ccschem.021.202101202
Corrected Citation: *CCS Chem.* **2022**, 4, 2588–2596
Previous Citation: *CCS Chem.* **2021**, 3, 2917–2921
Link to VoR: https://doi.org/10.31635/ccschem.021.202101202

Funding Information

Financial support from the National Key R&D Program of China (no. 2016YFC0700603), Natural Science Foundation of China (nos. 21631003 and 21805005), the Fundamental Research Funds for the Central Universities (nos. FRF-BD-20-14A and FRF-IDRY-19-028), and University of Science and Technology Beijing is gratefully acknowledged.

References

1. Cook, T. R.; Stang, P. J. Recent Developments in the Preparation and Chemistry of Metallacycles and Metallacages via Coordination. *Chem. Rev.* **2015**, *115*, 7001–7045.
2. Zhou, J.; Yu, G.; Huang, F. Supramolecular Chemotherapy Based on Host-Guest Molecular Recognition: A Novel Strategy in the Battle against Cancer with a Bright Future. *Chem. Soc. Rev.* **2017**, *46*, 7021–7053.
3. Jin, Y.; Zhang, Q.; Zhang, Y.; Duan, C. Electron Transfer in the Confined Environments of Metal-Organic Coordination Supramolecular Systems. *Chem. Soc. Rev.* **2020**, *49*, 5561–5600.
4. Dong, H.; Zhang, C.; Liu, X.; Yao, J.; Zhao, Y. Materials Chemistry and Engineering in Metal Halide Perovskite Lasers. *Chem. Soc. Rev.* **2020**, *49*, 951–982.
5. Fratini, S.; Nikolka, M.; Salleo, A.; Schweicher, G.; Sirringhaus, H. Charge Transport in High-Mobility Conjugated Polymers and Molecular Semiconductors. *Nat. Mater.* **2020**, *19*, 491–502.
6. Li, J.; Wang, J.; Li, H.; Song, N.; Wang, D.; Tang, B. Supramolecular Materials Based on AIE Luminogens (AIEgens): Construction and Applications. *Chem. Soc. Rev.* **2020**, *49*, 1144–1172.
7. He, X.; Hu, X.; James, T. D.; Yoon, J.; Tian, H. Multiplexed Photoluminescent Sensors: Towards Improved Disease Diagnostics. *Chem. Soc. Rev.* **2017**, *46*, 6687–6696.
8. Ogoshi, T.; Yamagishi, T.; Nakamoto, Y. Pillar-Shaped Macrocyclic Hosts Pillar[n]arenes: New Key Players for Supramolecular Chemistry. *Chem. Rev.* **2016**, *116*, 7937–8002.
9. Kolesnichenko, I. V.; Anslyn, E. V. Practical Applications of Supramolecular Chemistry. *Chem. Soc. Rev.* **2017**, *46*, 2385–2390.
10. Morimoto, M.; Bierschenk, S. M.; Xia, K. T.; Bergman, R. G.; Raymond, K. N.; Toste, F. D. Advances in Supramolecular Host-Mediated Reactivity. *Nat. Catal.* **2020**, *3*, 969–984.
11. Stefan, L.; Monchaud, D. Applications of Guanine Quartets in Nanotechnology and Chemical Biology. *Nat. Rev. Chem.* **2019**, *3*, 650–668.
12. Zhao, L.; Liu, Y.; Xing, R.; Yan, X. Supramolecular Photothermal Effects: A Promising Mechanism for Efficient Thermal Conversion. *Angew. Chem. Int. Ed.* **2020**, *59*, 3793–3801.
13. Lin, R.; He, Y.; Li, P.; Wang, H.; Zhou, W.; Chen, B. Multifunctional Porous Hydrogen-Bonded Organic Framework Materials. *Chem. Soc. Rev.* **2019**, *48*, 1362–1389.
14. Würthner, F.; Kaiser, T. E.; Saha-Möller, C. R. *J*-Aggregates: From Serendipitous Discovery to Supramolecular Engineering of Functional Dye Materials. *Angew. Chem. Int. Ed.* **2011**, *50*, 3376–3410.
15. Zhao, L.; Ren, X.; Yan, X. Assembly Induced Super-Large Red-Shifted Absorption: The Burgeoning Field of Organic Near-Infrared Materials. *CCS Chem.* **2021**, *3*, 678–693.
16. Proppe, A. H.; Li, Y. C.; Aspuru-Guzik, A.; Berlinguette, C. P.; Chang, C. J.; Cogdell, R.; Doyle, A. G.; Flick, J.; Gabor, N. M.; Grondelle, R. v.; Hammes-Schiffer, S.; Jaffer, S. A.; Kelley, S. O.; Leclerc, M.; Leo, K.; Mallouk, T. E.; Narang, P.; Schlau-Cohen, G. S.; Scholes, G. D.; Vojvodic, A.; Yam, V. W.; Yang, J. Y.; Sargent, E. H. Bioinspiration in Light Harvesting and Catalysis. *Nat. Rev. Mater.* **2020**, *5*, 828–846.
17. Breder, A.; Depken, C. Light-Driven Single-Electron Transfer Processes as an Enabling Principle in Sulfur and Selenium Multicatalysis. *Angew. Chem. Int. Ed.* **2019**, *58*, 17130–17147.
18. Xuan, J.; He, X.; Xiao, W. Visible Light-Promoted Ring-Opening Functionalization of Three-Membered Carbo- and Heterocycles. *Chem. Soc. Rev.* **2020**, *49*, 2546–2556.
19. Wang, C.; Dixneuf, P. H.; Soulé, J. Photoredox Catalysis for Building C-C Bonds from C(sp^2)-H Bonds. *Chem. Rev.* **2018**, *118*, 7532–7585.
20. Ghosh, I.; Ghosh, T.; Bardagi, J. I.; König, B. Reduction of Aryl Halides by Consecutive Visible Light-Induced Electron Transfer Processes. *Science* **2014**, *346*, 725–728.
21. Ghosh, I.; Shaikh, R. S.; König, B. Sensitization-Initiated Electron Transfer for Photoredox Catalysis. *Angew. Chem. Int. Ed.* **2017**, *56*, 8544–8549.
22. Jin, Y.; Wang, Q.; Taynton, P.; Zhang, W. Dynamic Covalent Chemistry Approaches toward Macrocycles, Molecular Cages, and Polymers. *Acc. Chem. Res.* **2014**, *47*, 1575–1586.
23. Jin, Y.; Yu, C.; Denman, R. J.; Zhang, W. Recent Advances in Dynamic Covalent Chemistry. *Chem. Soc. Rev.* **2013**, *42*, 6634–6654.
24. Hasell, T.; Cooper, A. I. Porous Organic Cages: Soluble, Modular and Molecular Pores. *Nat. Rev. Mater.* **2016**, *1*, 16053.
25. Mastalerz, M. Porous Shape-Persistent Organic Cage Compounds of Different Size, Geometry, and Function. *Acc. Chem. Res.* **2018**, *51*, 2411–2422.
26. Mukhopadhyay, R. D.; Kim, Y.; Koo, J.; Kim, K. Porphyrin Boxes. *Acc. Chem. Res.* **2018**, *51*, 2730–2738.
27. Moneypenny, T. P.; Walter, N. P.; Cai, Z.; Miao, Y.; Gray, D. L.; Hinman, J. J.; Lee, S.; Zhang, Y.; Moore, J. S. Impact of Shape Persistence on the Porosity of Molecular Cages. *J. Am. Chem. Soc.* **2017**, *139*, 3259–3264.
28. Wang, Q.; Luo, N.; Wang, X.; Ao, Y.; Chen, Y.; Liu, J.; Su, C.; Wang, D.; Wang, M. Molecular Barrel by a Hooping Strategy: Synthesis, Structure, and Selective CO_2 Adsorption Facilitated by Lone Pair-π Interactions. *J. Am. Chem. Soc.* **2017**, *139*, 635–638.
29. Qu, H.; Wang, Y.; Li, Z.; Wang, X.; Fang, H.; Tian, Z.; Cao, X. Molecular Face-Rotating Cube with Emergent Chiral and Fluorescence Properties. *J. Am. Chem. Soc.* **2017**, *139*, 18142–18145.
30. Furukawa, H.; Cordova, K. E.; ÓKeeffe, M.; Yaghi, O. M. The Chemistry and Applications of Metal-Organic Frameworks. *Science* **2013**, *341*, 1230444.

DOI: 10.31635/ccschem.021.202101202
Corrected Citation: *CCS Chem.* **2022**, 4, 2588–2596
Previous Citation: *CCS Chem.* **2021**, 3, 2917–2921
Link to VoR: https://doi.org/10.31635/ccschem.021.202101202

31. Xiao, J.; Jiang, H. Metal-Organic Frameworks for Photocatalysis and Photothermal Catalysis. *Acc. Chem. Res.* **2019**, *52*, 356–366.
32. Bai, Y.; Dou, Y.; Xie, L.; Rutledge, W.; Li, J.; Zhou, H. Zr-Based Metal-Organic Frameworks: Design, Synthesis, Structure, and Applications. *Chem. Soc. Rev.* **2016**, *45*, 2327–2367.
33. Li, B.; Wen, H.; Cui, Y.; Zhou, W.; Qian, G.; Chen, B. Emerging Multifunctional Metal-Organic Framework Materials. *Adv. Mater.* **2016**, *28*, 8819–8860.
34. Li, L.; Lin, R.; Krishna, R.; Li, H.; Xiang, S.; Wu, H.; Li, J.; Zhou, W.; Chen, B. Ethane/Ethylene Separation in a Metal-Organic Framework with Iron-Peroxo Sites. *Science* **2018**, *362*, 443–446.
35. Lin, S.; Diercks, C. S.; Zhang, Y.; Kornienko, N.; Nichols, E.; Zhao, Y.; Paris, A. R.; Kim, D.; Yang, P.; Yaghi, O. M.; Chang, C. J. Covalent Organic Frameworks Comprising Cobalt Porphyrins for Catalytic CO_2 Reduction in Water. *Science* **2015**, *349*, 1208–1213.
36. Slater, A. G.; Cooper, A. I. Function-Led Design of New Porous Materials. *Science* **2015**, *348*, aaa8075.
37. Wang, K.; Qi, D.; Li, Y.; Wang, T.; Liu, H.; Jiang, J. Tetrapyrrole Macrocycle Based Conjugated Two-Dimensional Mesoporous Polymers and Covalent Organic Frameworks: From Synthesis to Material Applications. *Coord. Chem. Rev.* **2019**, *378*, 188–206.
38. Feng, X.; Ding, X.; Jiang, D. Covalent Organic Frameworks. *Chem. Soc. Rev.* **2012**, *41*, 6010–6022.
39. Tan, C.; Jiao, J.; Li, Z.; Liu, Y.; Han, X.; Cui, Y. Design and Assembly of a Chiral Metallosalen-Based Octahedral Coordination Cage for Supramolecular Asymmetric Catalysis. *Angew. Chem. Int. Ed.* **2018**, *57*, 2085–2090.
40. Jiao, J.; Tan, C.; Li, Z.; Liu, Y.; Han, X.; Cui, Y. Design and Assembly of Chiral Coordination Cages for Asymmetric Sequential Reactions. *J. Am. Chem. Soc.* **2018**, *140*, 2251–2259.
41. Ronson, T.; League, A.; Gagliardi, L.; Cramer, C.; Nitschke, J. Pyrene-Edged $Fe^{II}_4L_6$ Cages Adaptively Reconfigure During Guest Binding. *J. Am. Chem. Soc.* **2014**, *136*, 15615–15624.
42. Hisaki, I.; Suzuki, Y.; Gomez, E.; Ji, Q.; Tohnai, N.; Nakamura, T.; Douhal, A. Acid Responsive Hydrogen-Bonded Organic Frameworks. *J. Am. Chem. Soc.* **2019**, *141*, 2111–2121.
43. Claassens, I. E.; Barbour, L. J.; Haynes, D. A. A Multistimulus Responsive Porous Coordination Polymer: Temperature-Mediated Control of Solid-State [2+2] Cycloaddition. *J. Am. Chem. Soc.* **2019**, *141*, 11425–11429.
44. Liu, Y.; Dai, J.; Guo, L.; Zhang, Z.; Yang, Y.; Yang, Q.; Ren, Q.; Bao, Z. Porous Hydrogen-Bonded Frameworks Assembled from Metal-Nucleobase Entities for Xe/Kr Separation. *CCS Chem.* **2021**, *3*, 1028–1035.
45. Liu, G.; Zhou, M.; Su, K.; Babarao, R.; Yuan, D.; Hong, M. Stabilizing the Extrinsic Porosity in Metal-Organic Cages-Based Supramolecular Framework by in Situ Catalytic Polymerization. *CCS Chem.* **2020**, *2*, 1382–1390.
46. Ding, M.; Jiang, H. Improving Water Stability of Metal-Organic Frameworks by a General Surface Hydrophobic Polymerization. *CCS Chem.* **2020**, *2*, 2740–2748.
47. Acharyya, K.; Mukherjee, P. S. Organic Imine Cages: Molecular Marriage and Applications. *Angew. Chem. Int. Ed.* **2019**, *58*, 8640–8653.
48. Mondal, B.; Mukherjee, P. S. Cage Encapsulated Gold Nanoparticles as Heterogeneous Photocatalyst for Facile and Selective Reduction of Nitroarenes to Azo Compounds. *J. Am. Chem. Soc.* **2018**, *140*, 12592–12601.
49. Zhang, C.; Wang, Q.; Long, H.; Zhang, W. A Highly C_{70} Selective Shape-Persistent Rectangular Prism Constructed through One-Step Alkyne Metathesis. *J. Am. Chem. Soc.* **2011**, *133*, 20995–21001.
50. McCaffrey, R.; Long, H.; Jin, Y.; Sanders, A.; Park, W.; Zhang, W. Template Synthesis of Gold Nanoparticles with an Organic Molecular Cage. *J. Am. Chem. Soc.* **2014**, *136*, 1782–1785.
51. Qiu, L.; McCaffrey, R.; Jin, Y.; Gong, Y.; Hu, Y.; Sun, H.; Park, W.; Zhang, W. Cage-Templated Synthesis of Highly Stable Palladium Nanoparticles and Their Catalytic Activities in Suzuki-Miyaura Coupling. *Chem. Sci.* **2018**, *9*, 676–680.
52. Yang, X.; Sun, J.; Kitta, M.; Pang, H.; Xu, Q. Encapsulating Highly Catalytically Active Metal Nanoclusters Inside Porous Organic Cages. *Nat. Catal.* **2018**, *1*, 214–220.
53. Sun, J.; Zhan, W.; Akita, T.; Xu, Q. Toward Homogenization of Heterogeneous Metal Nanoparticle Catalysts with Enhanced Catalytic Performance: Soluble Porous Organic Cage as a Stabilizer and Homogenizer. *J. Am. Chem. Soc.* **2015**, *137*, 7063–7066.
54. Han, B.; Wang, H.; Wang, C.; Wu, H.; Zhou, W.; Chen, B.; Jiang, J. Postsynthetic Metalation of a Robust Hydrogen-Bonded Organic Framework for Heterogeneous Catalysis. *J. Am. Chem. Soc.* **2019**, *141*, 8737–8740.
55. Wang, Z.; Sikdar, N.; Wang, S.; Li, X.; Yu, M.; Bu, X.; Chang, Z.; Zou, X.; Chen, Y.; Cheng, P.; Yu, K.; Zaworotko, M. J.; Zhang, Z. Soft Porous Crystal Based upon Organic Cages That Exhibit Guest-Induced Breathing and Selective Gas Separation. *J. Am. Chem. Soc.* **2019**, *141*, 9408–9414.
56. Sun, N.; Wang, C.; Wang, H.; Yang, L.; Jin, P.; Zhang, W.; Jiang, J. Multifunctional Tubular Organic Cage-Supported Ultrafine Palladium Nanoparticles for Sequential Catalysis. *Angew. Chem. Int. Ed.* **2019**, *58*, 18011–18016.
57. Slater, A. G.; Little, M. A.; Pulido, A.; Chong, S. Y.; Holden, D.; Chen, L.; Morgan, C.; Wu, X.; Cheng, G.; Clowes, R.; Briggs, M. E.; Hasell, T.; Jelfs, K. E.; Day, G. M.; Cooper, A. I. Reticular Synthesis of Porous Molecular 1D Nanotubes and 3D Networks. *Nat. Chem.* **2016**, *9*, 17–25.
58. Zhang, C.; Wang, Z.; Tan, L.; Zhai, T. L.; Wang, S.; Tan, B.; Zheng, Y. S.; Yang, X. L.; Xu, H. B. A Porous Tricyclooxacalixarene Cage Based on Tetraphenylethylene. *Angew. Chem. Int. Ed.* **2015**, *54*, 9244–9248.
59. Yu, G.; Cen, T. Y.; He, Z.; Wang, S. P.; Wang, Z.; Ying, X. W.; Li, S.; Jacobson, O.; Wang, S.; Wang, L.; Lin, L. S.; Tian, R.; Zhou, Z.; Ni, Q.; Li, X.; Chen, X. Porphyrin Nanocage-Embedded Single-Molecular Nanoparticles for Cancer Nanotheranostics. *Angew. Chem. Int. Ed.* **2019**, *58*, 8799–8803.
60. Bi, S.; Thiruvengadam, P.; Wei, S.; Zhang, W.; Zhang, F.; Gao, L.; Xu, J.; Wu, D.; Chen, J.; Zhang, F. Vinylene-Bridged Two-Dimensional Covalent Organic Frameworks via Knoevenagel Condensation of Tricyanomesitylene. *J. Am. Chem. Soc.* **2020**, *142*, 11893–11900.

DOI: 10.31635/ccschem.021.202101202
Corrected Citation: *CCS Chem.* **2022**, 4, 2588–2596
Previous Citation: *CCS Chem.* **2021**, 3, 2917–2921
Link to VoR: https://doi.org/10.31635/ccschem.021.202101202

61. Zou, Y.; Chen, J.; Liu, X.; Lu, L.; Davis, R. L.; Jørgensen, K. A.; Xiao, W. Highly Efficient Aerobic Oxidative Hydroxylation of Arylboronic Acids: Photoredox Catalysis Using Visible Light. *Angew. Chem. Int. Ed.* **2012**, *51*, 784–788.
62. Tang, B.; Xu, W.; Xu, J.; Zhang, X. Transforming a Fluorochrome to an Efficient Photocatalyst for Oxidative Hydroxylation: A Supramolecular Dimerization Strategy Based on Host-Enhanced Charge Transfer. *Angew. Chem. Int. Ed.* **2021**, *60*, 9384–9388.
63. Qian, Y.; Li, D.; Han, Y.; Jiang, H. Photocatalytic Molecular Oxygen Activation by Regulating Excitonic Effects in Covalent Organic Frameworks. *J. Am. Chem. Soc.* **2020**, *142*, 20763–20771.
64. Wei, P.; Qi, M.; Wang, Z.; Ding, S.; Yu, W.; Liu, Q.; Wang, L.; Wang, H.; An, W.; Wang, W. Benzoxazole-Linked Ultrastable Covalent Organic Frameworks for Photocatalysis. *J. Am. Chem. Soc.* **2018**, *140*, 4623–4631.
65. Liu, C.; Liu, K.; Wang, C.; Liu, H.; Wang, H.; Su, H.; Li, X.; Chen, B.; Jiang, J. Elucidating Heterogeneous Photocatalytic Superiority of Microporous Porphyrin Organic Cage. *Nat. Commun.* **2020**, *11*, 1047.

DOI: 10.31635/ccschem.021.202101202
Corrected Citation: *CCS Chem.* **2022**, 4, 2588–2596
Previous Citation: *CCS Chem.* **2021**, 3, 2917–2921
Link to VoR: https://doi.org/10.31635/ccschem.021.202101202